Cross-Polarization Gain Calibration of Linearly Polarized VLBI Antennas by Observations of 4C 39.25

Radio Science®

RESEARCH ARTICLE
10.1029/2023RS007892

Cross-Polarization Gain Calibration of Linearly Polarized VLBI Antennas by Observations of 4C 39.25

F. Jaron[1,2], I. Martí-Vidal[3,4], M. Schartner[5], J. González-García[6], E. Albentosa-Ruiz[4], S. Bernhart[2,7,8], J. Böhm[1], J. Gruber[1], S. Modiri[8], A. Nothnagel[1], V. Pérez-Díez[6,9], T. Savolainen[2,10,11], B. Soja[5], E. Varenius[12], and M. H. Xu[10,13]

[1]Technische Universität Wien, Wien, Austria, [2]Max-Planck-Institut für Radioastronomie, Bonn, Germany, [3]Departament d'Astronomia i Astrofísica, Universitat de València, València, Spain, [4]Observatori Astronòmic, Universitat de València, Parc Científic, València, Spain, [5]Institute of Geodesy and Photogrammetry, ETH Zürich, Zürich, Switzerland, [6]Centro Astronómico de Yebes (IGN), Yebes, Spain, [7]Reichert GmbH, Bonn, Germany, [8]Department Geodesy, Federal Agency for Cartography and Geodesy (BKG), Frankfurt am Main, Germany, [9]Observatorio Astronómico Nacional (OAN-IGN), Madrid, Spain, [10]Aalto University Metsähovi Radio Observatory, Kylmälä, Finland, [11]Aalto University Department of Electronics and Nanoengineering, Aalto, Finland, [12]Chalmers University of Technology, Gothenburg, Sweden, [13]GFZ German Research Centre for Geosciences, Potsdam, Germany

Key Points:

- The new-generation geodetic radio telescopes observe two orthogonal linear polarization directions
- Calibration of the gain differences between the two polarizers is necessary to maximize the signal-to-noise ratio of observations
- We investigate these cross-polarization gain differences and their temporal evolution for selected antennas

Correspondence to:

F. Jaron,
frederic.jaron@tuwien.ac.at

Citation:

Jaron, F., Martí-Vidal, I., Schartner, M., González-García, J., Albentosa-Ruiz, E., Bernhart, S., et al. (2024). Cross-polarization gain calibration of linearly polarized VLBI antennas by observations of 4C 39.25. *Radio Science*, *59*, e2023RS007892. https://doi.org/10.1029/2023RS007892

Received 19 OCT 2023
Accepted 29 FEB 2024

Abstract Radio telescopes with dual linearly polarized feeds regularly participate in Very Long Baseline Interferometry. One example is the VLBI Global Observing System (VGOS), which is employed for high-precision geodesy and astrometry. In order to achieve the maximum signal-to-noise ratio, the visibilities of all four polarization products are combined to Stokes *I* before fringe-fitting. Our aim is to improve cross-polarization bandpass calibration, which is an essential processing step in this context. Here we investigate the shapes of these station-specific quantities as a function of frequency and time. We observed the extra-galactic source 4C 39.25 for 6 hours with a VGOS network. We correlated the data with the DiFX software and analyzed the visibilities with PolConvert to determine the complex cross-bandpasses with high accuracy. Their frequency-dependent shape is to first order characterized by a group delay between the two orthogonal polarizations, in the order of several hundred picoseconds. We find that this group delay shows systematic variability in the range of a few picoseconds, but can remain stable within this range for several years, as evident from earlier sessions. On top of the linear phase-frequency relationship there are systematic deviations of several tens of degrees, which in addition are subject to smooth temporal evolution. The antenna cross-bandpasses are variable on time scales of ∼1 hr, which defines the frequency of necessary calibrator scans. The source 4C 39.25 is confirmed as an excellent cross-bandpass calibrator. Dedicated surveys are highly encouraged to search for more calibrators of similar quality.

1. Introduction

Antennas participating in Very Long Baseline Interferometry (VLBI) have traditionally been observing with circularly polarized feeds (Thompson et al., 2017). New developments make it necessary that antennas also observe in linear polarization. One such example, and the subject of this paper, is the VLBI Global Observing System (VGOS, Petrachenko et al., 2009, still under the name of "VLBI2010"). Aimed at improving the precision of geodetic and astrometric VLBI (Sovers et al., 1998) down to mm and sub-mm/year scales, it was recognized that this requires an extension of the observed bandwidth to the range of 2–15 GHz. Such a bandwidth is best realized with the use of linear feeds, because $\lambda/4$-plates, necessary for the realization of circular polarization, do not work over such a large frequency range. See, however, Abdalmalak et al. (2020) for the possibility of using circularly polarized log-spiral antennas for reception and Jaradat et al. (2021) for emission of broadband radio signals.

Using linear feeds requires that the telescopes simultaneously observe two perpendicular polarization directions. Throughout this paper, we are going to refer to these polarization directions as "H" for horizontal and "V" for vertical. In the context of VGOS, these polarization directions are also referred to as "X" and "Y." However, this terminology is invalid because the linear feeds of VGOS antennas are not aligned with celestial coordinate axes. Two polarization directions are necessary because non-zero parallactic angle differences between the telescopes of long baselines generally cause a loss of signal-to-noise ratio (SNR) of the parallel hand polarization products. In order to obtain the full SNR for all parallactic angles it is necessary to combine all four polarization products

with each other to form Stokes I for fringe-fitting. The formula for Stokes I_{ab} for a baseline consisting of telescopes a and b is

$$I_{ab} = \left(H_a H_b + \rho_a \rho_b^* V_a V_b\right) \cos \Delta + \left(\rho_b^* H_a V_b - \rho_a V_a H_b\right) \sin \Delta, \quad (1)$$

where the terms H_aH_b and V_aV_b are the "parallel-hand" linear polarization correlation products (i.e., visibilities), and H_aV_b and V_aH_b and the "cross-hand" products. The coefficients $\rho_{a,b}$ denote the complex gain differences between the H and V polarizers at each antenna a and b, in terms of amplitude A and phase φ, that is, $\rho = Ae^{i\varphi}$. Finally, Δ is the parallactic angle difference between the antennas a and b. Obviously, for the realization of coherent summation of the correlator visibilities, the computation of Stokes I requires information about the complex gain differences ρ between the two linear feeds of each antenna participating in the observation. We will refer to this quantity, which is a function of frequency over the observed bandwidth, as the *cross-polarization bandpass* (or simply *cross-bandpass*). The investigation of the cross-bandpasses, both as a function of frequency and time, that is, $\rho(\nu, t)$, is the subject of this article. Equation 1 makes it evident that well-determined cross-polarization bandpasses are a key quantity for any VLBI experiments in which linearly polarized antennas participate.

Cross-bandpass calibration is a processing step that is commonly carried out for each VGOS session after correlation and before final fringe-fitting. The approach that is currently being applied is to use observations of the session to be processed also for the determination of the cross-bandpasses. One procedure, developed at MIT Haystack Observatory, applying the program `fourfit`, is described in Niell et al. (2018), and has become the generally adopted method for the processing of VGOS experiments (A detailed description of the procedure can be found in this document: https://www.haystack.mit.edu/wp-content/uploads/2020/07/docs_hops_000_vgos-data-processing.pdf, accessed on 2 October 2023, as all other links in this article). However, the software `PolConvert` (Martí-Vidal et al., 2016) offers an alternative route for VGOS data processing. For the investigations at hand, we make use of the capability of PolConvert to estimate the cross-polarization gains with configurable spectral resolution and time averaging.

The principal functionality of `PolConvert` is to convert visibilities of linearly polarized data to a circularly polarized basis. For optimal results, cross-polarization bandpass calibration is an essential processing step. Compared to the cross-bandpass calibration implemented in the Haystack Observatory Postprocessing System (HOPS), the algorithm in `PolConvert` is potentially superior, because it makes use of both amplitude and phase of the visibilities, and also offers the possibility to use the instrumental phase-calibration signal ("phase-cal") to determine delays between H and V polarization. The code performs a least-squares fitting of the visibility data directly without fringe-fitting. `PolConvert` has been used to convert ALMA observations from linear to circular for the Event Horizon Telescope (Event Horizon Telescope Collaboration et al., 2019) and also for the Global mm-VLBI Array (Zhao et al., 2022). However, in both of these cases, the cross-bandpasses were calibrated using pre-determined calibration tables. The applicability of `PolConvert` to VGOS data has been demonstrated by Alef, Tuccari, et al. (2019) and further described by Martí-Vidal et al. (2021), in which case the cross-bandpasses are determined from calibration scans. The different processing steps of `PolConvert` can be run separately. Here we make use of the step that determines the cross-polarization gains as a tool to estimate these quantities for the analysis presented in this article.

Because cross-polarization bandpass calibration is a crucial step in the VGOS processing chain, the aim of our investigation is to measure and characterize the cross-bandpasses of VGOS antennas. For an optimal measurement, two requirements are of essential importance. Firstly, the observed radio source has to be a suitable calibrator. Prior to our investigations presented here, we examined a number of calibrator scans that were observed as part of research and development (R&D) sessions of the EU-VGOS project (Albentosa et al., 2023; Alef, Anderson, et al., 2019; Jaron et al., 2021). An inspection of the cross-bandpass solutions from multiple calibrator scans has revealed that there are huge differences in their quality and that there is an obvious dependency on the observed source. There is one source for which the results stand out compared to other sources, and this is the radio-loud active galactic nucleus (AGN) 4C 39.25. Secondly, the observing geometry is critical, in particular the coverage of the parallactic angle. For the research presented here, we designed a session that uses this knowledge for the optimal measurement of the cross-bandpasses of the VGOS antennas that participated in our observations.

Table 1
List of Stations Included in the Schedule for the Session er2201

Code	Name	Description	Comment
Mg	MACGO12 M	McDonald Geodetic Observatory (MGO), TX, USA	[a]
Oe	ONSA13NE	Onsala 13-m antenna north-east, Sweden	
Ow	ONSA13SW	Onsala 13-m antenna south-west, Sweden	
Wf	WESTFORD	Westford, MA, USA	
Ws	WETTZ13S	Wettzell 13-m antenna south, Germany	
Yj	RAEGYEB	13-m at Yebes, Spain	[b]

[a]For Mg, data only partly available after 2 hr. [b]Yj did not observe VGOS band D.

Another possibility of realizing dual circular polarization for broadband receivers, such as VGOS, is the use of so-called 3 dB/90° microwave hybrid couplers. These devices offer a hardware solution to convert dual linear into dual circular polarization, and can be installed at the telescopes before the low-noise amplifiers. Their potential suitability for VGOS has been described in a technical report (García-Pérez, Terceroc, Malo, & López-Pérez, 2018). In another technical report García-Pérez, Terceroc, Malo, Gallego, and López-Pérez (2018) discuss these devices as a possibility for the BRAND receiver (Alef, Anderson, et al., 2019). In the time of writing, the only VGOS observing mode that has so far been carried out is to record the data in linear polarization and account for this during the digital data processing after correlation, and we are going to assume this mode in the remainder of this article. It is important to note that also in the case that the data are recorded in dual circular polarization, if ones wants to combine the data to Stokes *I*, it is still necessary to determine the cross-polarization bandpass (between R and L) and to properly calibrate the data. Also, an additional device, such as a hybrid coupler, comes at the risk of introducing additional systematic errors (as discussed in the two technical reports mentioned) and degrading the signal-to-noise ratio. For these reasons, we tentatively conclude that for broadband observations the use of dual linear polarization along with a software solution is the better option. However, we strongly encourage experiments to test observing with hybrid couplers. More information about hybrid couplers can be found in a number of publications (Khudchenko et al., 2019; Kooi et al., 2023; López-Pérez et al., 2021; Malo-Gomez et al., 2009).

The paper is organized as follows. We give a brief introduction to the astrophysical object 4C 39.25 in Section 2. In Section 3 we describe the properties of our VGOS R&D session. We describe our methods in Section 4 and present our results in Section 5. We give our conclusions in Section 6.

2. The Source 4C 39.25

During the inspection of the results of cross-bandpass calibration from different scans that were initially scheduled for this purpose in previous sessions, it turned out that the quality of the results was variable and that there was an apparent dependency on the radio source under observation. Among the many sources that were each observed multiple times with 2–3 min scans, one source always stood out in terms of cleanliness of the cross-bandpass solution, and that was 4C 39.25. For this reason, we have chosen this source as the target for our dedicated experiment with the aim of measuring and investigating the cross-bandpasses of VGOS antennas.

Discovered during a survey of radio sources (Pilkington & Scott, 1965), 4C 39.25 (B1950 name 0923 + 392) soon became a target of astrophysical interest. Linear polarization of its radio emission was detected (Aller, 1970; Berge & Seielstad, 1969), and Bignell and Seaquist (1973) even published a time-series of polarization. Nartallo et al. (1998) classify the source as a "low polarization quasar" (see their Table 2), referring to the research by Impey and Tapia (1990). Indeed, Impey and Tapia (1990) report a polarization of $p = 0.5 \pm 0.5$, which indicates that p is equal to zero, that is, that the source is not polarized. However, this value has been derived for the optical emission from this source (see their Table 1). In the same article, the authors also come to the conclusion that optical and radio polarization are not correlated, which in turn means that it cannot be ruled out that the radio emission from 4C 39.25 could still be polarized to some degree. Alberdi et al. (2000) present VLBI observations at 15, 22, and 43 GHz, showing that features in the jet are polarized while the component that they interpret as the core is not polarized at radio wavelengths. In addition to that, Alberdi et al. (2000) report some features in the jet

Table 2
Frequency Setup

Band	Min. freq.	IF upper bounds [MHz]							
A	3,000.4	3,032.4	3,064.4	3,096.4	3,224.4	3,320.4	3,384.4	3,448.4	3,480.4
B	5,240.4	5,272.4	5,304.4	5,336.4	5,464.4	5,560.4	5,624.4	5,688.4	5,720.4
C	6,360.4	6,392.4	6,424.4	6,456.4	6,584.4	6,680.4	6,744.4	6,808.4	6,840.4
D	10,200.4	10,232.4	10264.4	10,296.4	10,424.4	10,520.4	10,584.4	10,648.4	10,680.4

Note. The four VGOS bands are labeled A–D, each has a bandwidth of 480 MHz with a frequency range as given in the table. Each band is further divided into eight IF sub-bands with a bandwidth of 32 MHz each, the upper bounds of which are given in the table.

to move at apparently superluminal speeds, implying that Doppler boosting of the intrinsic emission plays an important role for this source. The source is also in the MOJAVE Survey (see https://www.cv.nrao.edu/MOJAVE/sourcepages/0923+392.shtml).

3. The VLBI Session er2201

For the purpose of measuring the cross-bandpasses of VGOS antennas, we carried out a dedicated R&D session. The principal idea was to observe 4C 39.25, which we had identified as an excellent cross-bandpass calibrator, for 6 hours. Here we describe the details of this session, which was carried out under the name er2201.

3.1. Scheduling

The scheduling for the session er2201 was performed with the software VieSched++ (Schartner & Böhm, 2019). The session was observed on 8 September 2022, from 11:30 to 17:30 UTC. The network consisted of the VGOS stations Mg, Oe, Ow, Wf, Ws, and Yj. Details about the stations are given in Table 1.

The frequency setup of our observation is identical to the one currently used for global VGOS sessions (Niell et al., 2018) and is listed in Table 2. We follow the convention of the VGOS community and label the four bands with letters A, B, C, D. Each of these bands has a frequency range of 480 MHz and is further divided into eight sub-bands of 32 MHz bandwidth each. All of these sub-bands are realized as lower side-bands, which is why the upper bounds of these bands are given in Table 2. A visualization of the frequency setup can be seen in Figure 1. The frequency spans of the four VGOS bands are presented by the gray-shaded areas, and the distributions of the sub-bands within these bands are shown as black areas.

The session started with two 5-min scans of the two radio-loud AGNs NRAO150 and OJ287. These scans were included in the schedule with the aim of investigating the potential suitability of other sources as cross-bandpass calibrators. These two sources were chosen because they were also giving good results in the past, albeit not as good as 4C 39.25. The remainder of the session consists of a series of repeated 10-min scans on 4C 39.25. In order to give the electronics at the stations the time to reset, gaps of duration 5 s were scheduled in between scans.

Cross-polarization bandpass calibration requires a large enough parallactic angle coverage. In principle, it is possible to determine the amplitudes and phases of the cross-gains within a few minutes of observation if the parallactic angle of one antenna changes fast enough. In practice this means that it is sufficient that one antenna of the network of a scan observes the source with a large elevation angle; ideally, the source would be observed *in*

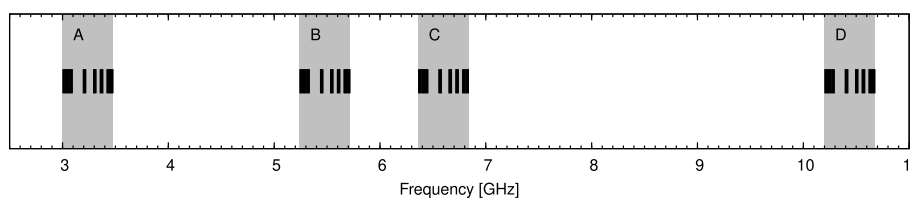

Figure 1. Frequency setup of our observations. The letters A, B, C, and D refer to the VLBI Global Observing System band labels. See Table 2 for details.

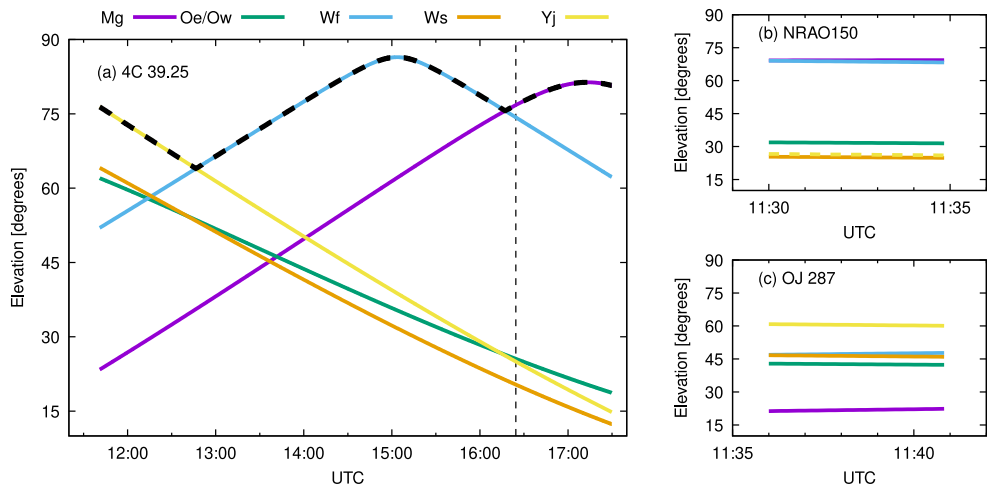

Figure 2. Antenna elevations as a function of time for day 2022-09-08. (a) Observations of 4C 39.25. The position of scan 143 (reference scan) is marked by the dashed vertical line at 16:24 UTC. The dashed curves highlight the upper envelope of elevations. (b) Elevations for the observation of NRAO150. Station Yj missed this scan as indicated by the dash line. (c) Elevations for the observation of OJ287.

transit. Our scheduling approach was thus to search for a 6-hr time window, within the 24 hr of a day, during which a network of VGOS telescopes could observe our target source 4C 39.25 such that one antenna in each scan always has a large elevation angle. In Figure 2, panels (a) to (c) show the elevation angle of each antenna as a function of time. The plot in panel (a) refers to observations of the main target 4C 39.25. The elevation angle of the two other candidate sources, observed in the beginning of the session, are plotted in the two panels of the right-hand side, observations of NRAO 150 in panel (b) and OJ 287 in panel (c).

The fact that a high elevation angle of one participating antenna is crucial for the quality of the cross-bandpass solution means that an important quantity is the upper envelope of the elevation plot shown in Figure 2a. This upper envelope is plotted as the black dashed line. It is made up of the curves for station Yj from the beginning until ∼12:45. After that Wf takes over and has the highest elevation of the network until about 16:15, when this role is given to station Mg until the end of the session. The importance of these stations during these observational time spans should be kept in mind in the context of data issues, as explained further down in the text.

How large should the elevation angle of an antenna be to guarantee a large enough parallactic angle coverage? The left-hand panel of Figure 3 shows the parallactic angle of each antenna as a function of observation time. Color coding, time range, and source are the same as in Figure 2, allowing a direct comparison of the two figures. Indeed, there is a correspondence of steep slopes of the parallactic angles in left-hand panel of Figure 3 during times of high elevations in Figure 2a. This is particularly evident for station Wf, which has an elevation of almost 90° at around 15:00 UTC, resulting in a very high slope of parallactic angle during the same time. A similar

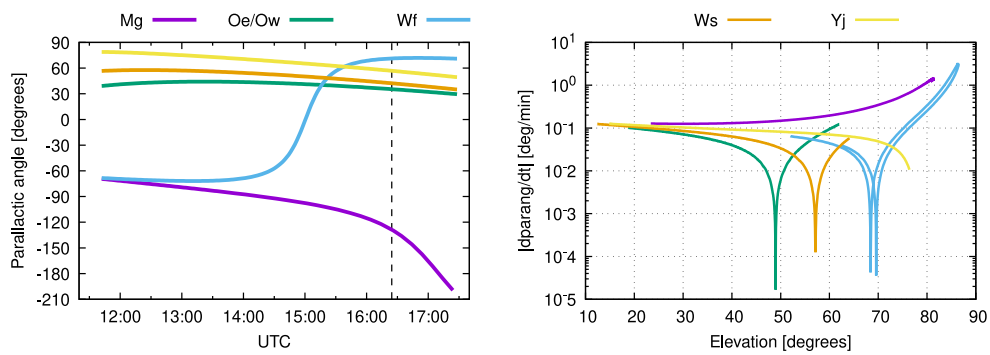

Figure 3. Left: Parallactic angle against observation time. Right: Absolute value of the time derivative of the parallactic angle, plotted against elevation angle.

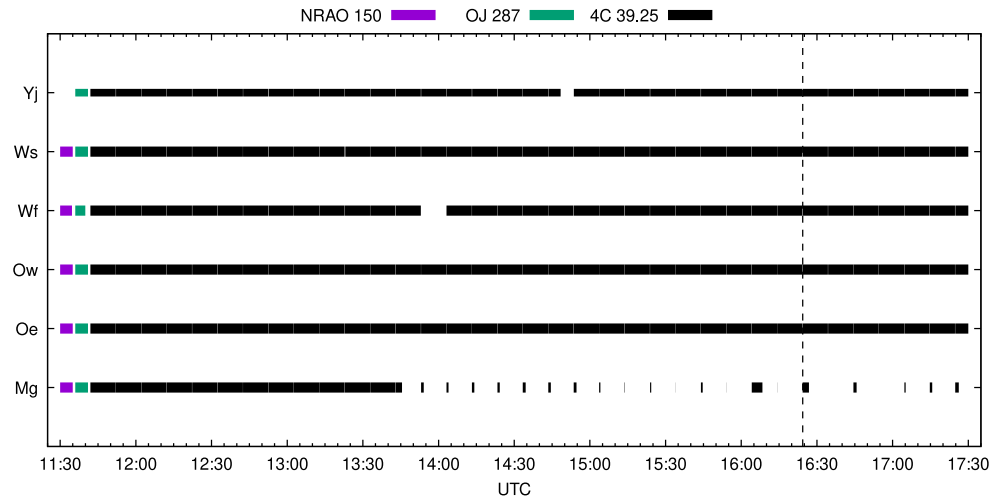

Figure 4. Observation times and data availability of the participating stations. The session er2201 lasted from 11:30 until 17:30 UTC on 8 September 2022. For station Mg data from 13:43 on are only partly available. The line for station Yj appears thinner than the lines for the other stations to indicate that Yj did not record the full bandwidth, missing VLBI Global Observing System band D. The vertical dashed line marks the position of scan 143, which serves as the reference scan.

correspondence can be seen for station Mg around 17:00 UTC. To investigate the dependency between elevation and parallactic angle coverage in more detail, the right-hand panel of Figure 3 presents the absolute value of the time derivative of the parallactic angle, plotted against the elevation angle for each antenna. The *y*-axis has a logarithmic scale and is given in units of degrees per minute. And indeed, parallactic angle rates of several degrees per minute are reached for elevation angles above ∼80° for station Mg and for elevation angles above ∼85° for station Wf. However, the elevation dependency is not so simple in the sense that a larger elevation angle automatically means a larger parallactic angle coverage. Based on this plot, an elevation angle larger than approximately 80°–85° should guarantee a parallactic angle coverage of several degrees in a single scan with a duration of a few minutes, which is enough to break the degeneracy in the system of equations to compute the complex cross-polarization bandpass.

3.2. The Data

Figure 4 presents a plot showing the observing times of each station that participated in er2201. As indicated by the line colors, two candidate sources were observed at the beginning of the session: NRAO150 (purple) and OJ 287 (green). For the remainder of the session, the source 4C 39.25 (black) was observed exclusively.

Two stations had issues during the session. Yj missed the first scan to the source NRAO150, and throughout the entire session, this station did not record the VGOS band D. This fact is indicated by the line width, which is thinner for this station than for the other stations. Station Yj is responsible for the highest elevation angles in the beginning of the session until about 12:45, which should be kept in mind when interpreting results.

The other major issue occurred at station Mg. For the first 2 hours of the session, the data from this station are fully available. But then starting at 13:43 UTC only fractions of the scheduled scan lengths are available. This fact corresponds to the sparsity of the line in Figure 4 for that station from that moment on. The reason for this data loss has been identified to be a software issue used in combining the data that has been fixed (Chet Ruszczyk, MIT Haystack Observatory, priv. comm.). There is, however, unfortunately no way to recover these data anymore for the original data was deleted. The missing data for Mg, especially during the later times of this session, is a matter of concern because Mg marks the upper envelope of the elevation plot from about 16:15 on (see the dashed line in Figure 2a).

Besides these two major issues, only two gaps appear in the data for Yj (∼14:40, where only data for VGOS band A are missing) and Wf (∼14:00, all bands missing). Otherwise we have a solid database to analyze from this session.

Table 3
`PolConvert` *Processing Steps*

	Description
0	Source scanner (Initial fringe-fitting, SNR estimate)
1	Estimate cross-polarization gains
2	PolConvert the whole experiment
3	Estimate additive phases and write fourfit control file
4	Calibrate bandpass and remove IONEX TEC (optional)
5	Perform broadband Global Fringe Fitting (optional)
6	Write fully calibrated SWIN files

4. Methods

The data processing for our present work consists of correlation of the raw observational data and analysis of the resulting visibilities with the software `PolConvert`. Here we describe our methods.

4.1. Correlation

The data were correlated at the VLBI correlator of the Technical University of Vienna (TU Wien), making use of the Vienna Scientific Cluster (VSC4, https://vsc.ac.at/systems/vsc-4/). We used the DiFX software correlator (Deller et al., 2011) in its version 2.5.4, which is the current version to be used for the correlation of VGOS data (Jaron et al., 2021). For the analysis of the present work, we divided the original 10-min scans into slices of 2-min by editing the vex control file. We then correlated the data with a spectral resolution of 250 kHz (i.e., 128 channels per sub-band of bandwidth 32 MHz) with a length of the accumulation periods of 1 s.

4.2. Cross-Polarization Bandpass Calibration

We use the `PolConvert` software (Martí-Vidal et al., 2016, 2021) for the determination of the cross-bandpasses. In its current version, `PolConvert` distinguishes seven processing steps (numbered 0 to 6), as listed in Table 3. These steps can be run individually.

Step number 0 ("Source scanner") carries out an initial fringe-fitting of each scan in order to estimate the signal-to-noise ratio (SNR). In the masterfile (a Python script that serves as the user interface to `PolConvert`) one can configure the sub-bands to be included in the fringe-fitting. For our present analysis, we include all 32 sub-bands. In the output file of step 0, `PolConvert` reports the information on whether a scan is suitable for the estimation of the cross-gains along with detailed information about the SNR of each antenna and sub-band.

In step 1 the cross-polarization bandpasses are estimated as a complex quantity, that is, the complex gain differences between the two polarizers as a function of frequency for each antenna. The user has the possibility to configure how many spectral channels the algorithm averages and the integration time. For the data of our experiment, it turns out that averaging over eight channels and an integration time of 20 s gives the best results. We use `PolConvert` step 1 with this configuration for the estimation of the cross-polarization bandpasses presented further down in this article. For this step, and for all of the subsequent analyses, we exclude the very short baseline between the Onsala twin telescopes. The reason for this is that, because of the constantly very low fringe rate on this baseline, the phase-cal signal always interferes and dominates the cross-power spectrum. Flagging of the affected channels would be another means of mitigating this problem, but we choose to eliminate this baseline altogether in order to avoid any contamination at all.

Step 2 converts the visibilities for the entire experiment from linear to circular polarization. It uses the results from step 1 for the calibration of the complex cross-polarization gain differences between the two linear feeds of each antenna. Residual phase-offsets between sub-bands are corrected for in `PolConvert` step 3, which writes a `Fourfit` control file containing the corresponding phase corrections. It can be used for the final fringe-fitting of the data with the HOPS `Fourfit` program. The last three steps are not used for the analysis presented in this article. We are just listing them here for completeness.

5. Results

Here we present the results from our analysis of the visibilities to estimate the cross-polarization bandpasses of the participating stations, using the software `PolConvert` (Martí-Vidal et al., 2016), as described in the previous section. First, we investigate the dependency of amplitude and phase of the cross-bandpasses as a function of frequency (Section 5.1), then we explore their evolution with time (Section 5.2).

An eye-inspection of the results for the 175 2-min scans made it evident that, while most of the estimated cross-bandpasses are of high quality, safe for a few outliers, the solutions of the individual scans still differ in quality. We came to the conclusion that scan number 143 yields a solution that can serve as a reference for a good example. The scan refers to an observation of the source 4C 39.25 at 16:24 UTC and includes data from all

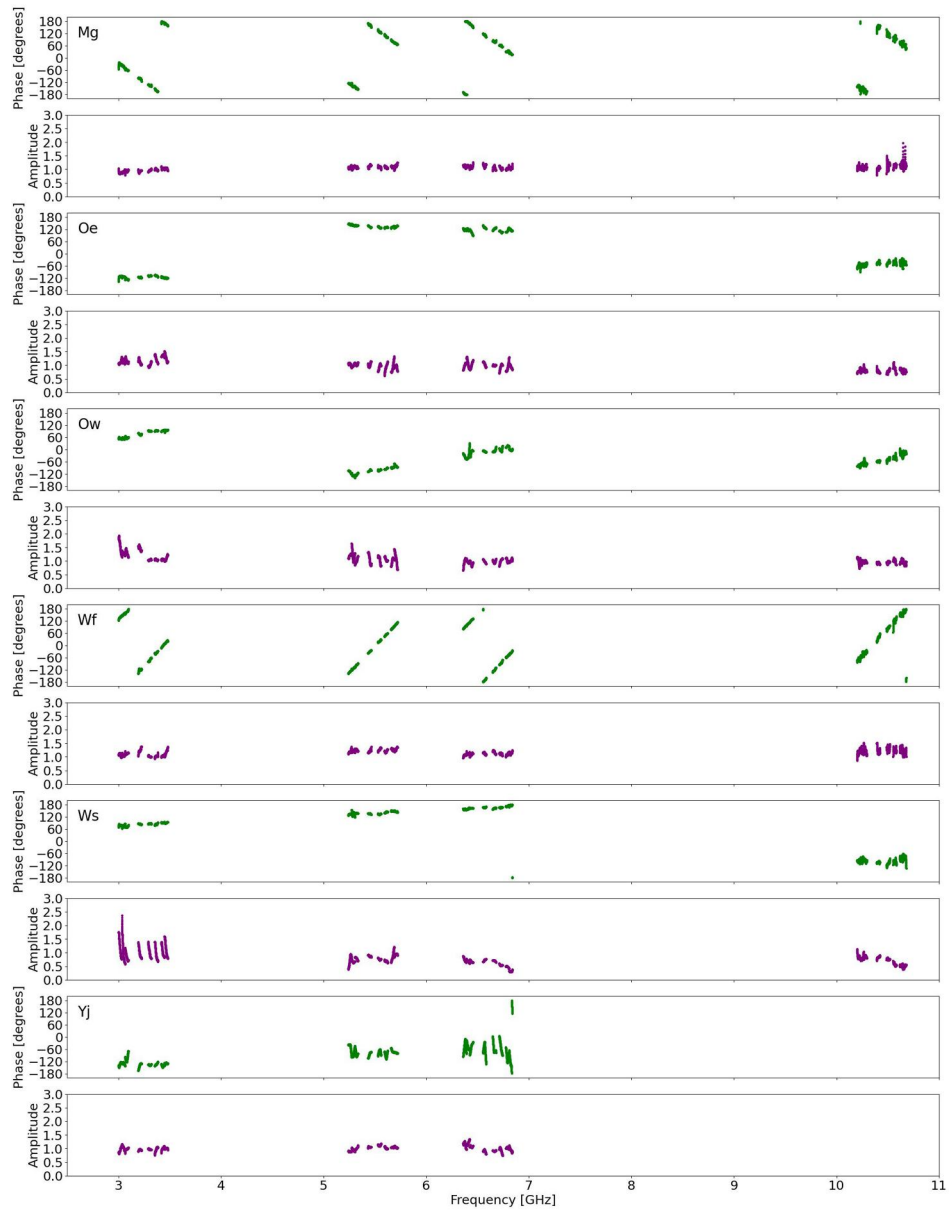

Figure 5. Cross-polarization bandpass of all stations, see Section 5.1 for details, resulting from analyzing scan 143 (the reference scan). For each station as labeled in the upper-left corner there is a pair of two panels: the upper panel shows the phases (green points), and the bottom one shows amplitude (purple points). Both amplitude and phase are plotted against frequency.

stations. The position of this scan is marked by the vertical dashed line in Figures 2 and 4, and we will refer to this scan as the *reference scan* in the remainder of the text.

5.1. Frequency-Dependency

Figure 5 shows the cross-polarization bandpasses, determined by analyzing reference scan 143 with `PolConvert`. This serves as an example of how cross-bandpasses typically look like. The figure shows, from top to bottom, the solutions in terms of amplitude (purple) and phase (green) plotted against frequency for all stations participating in this experiment.

For all stations, amplitude and phase are not constant over the full bandwidth but are subject to considerable variability as a function of frequency. In the following, we select Onsala West as an example station to analyze the

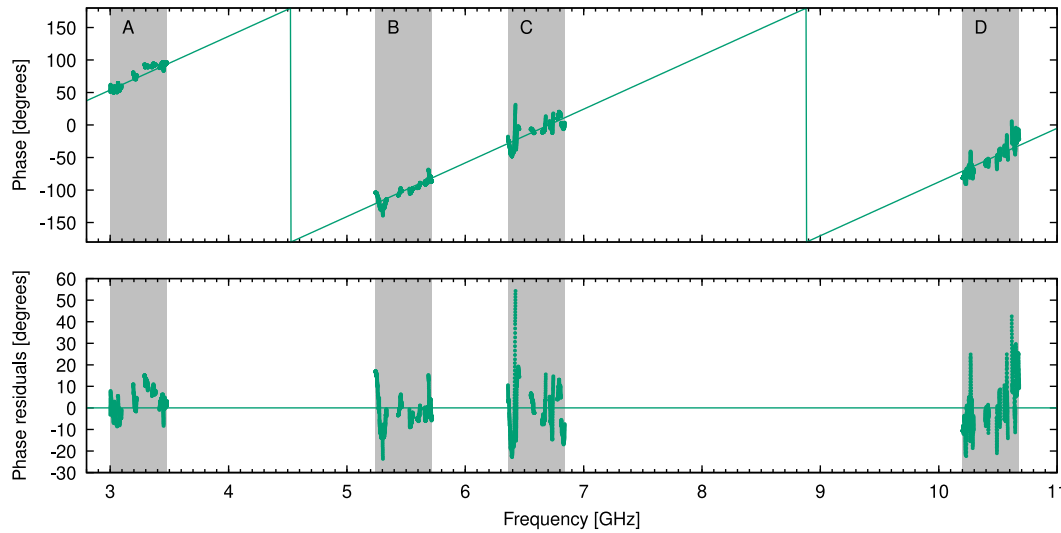

Figure 6. Top: Cross-polarization bandpass of the VLBI Global Observing System (VGOS) antenna Onsala West over the full frequency range. The solid line is a functional fit to the data. Bottom: Residuals, that is, measured phases minus model phases. Gray-shaded areas highlight the frequency ranges of the VGOS bands, as indicated by the labels.

frequency-dependency of the phases in more detail and in a quantitative way. The top panel of Figure 6 shows the cross-gain phases for station Onsala West plotted against frequency for the full observed bandwidth. It is obvious that to first order the phases follow a linear trend with frequency. The physical interpretation of this is that there is a group delay between the two linear feeds of the antenna. We fit the phase φ as a function of the frequency ν of the form

$$\varphi(\nu) = \mathrm{fmod}\big(360\nu\tau + \varphi_0, 360\big) - 180°, \tag{2}$$

where τ is the group delay and φ_0 is the phase offset. The function fmod(x, y) returns the floating-point remainder of the division x/y, as implemented in the `Python` math package. We use the `Python` iminuit package to fit this function to the data. The result is

$$\tau = 230 \pm 0.2 \text{ ps}, \tag{3}$$

$$\varphi_0 = -14.1° \pm 0.4°, \tag{4}$$

and is plotted as the solid line in the upper panel of Figure 6. This result means that there is an overall time delay between the two linear receivers, with the signal from the V polarization arriving about 230 ps later than the signal from the H polarization. We will come back to this fit and its evolution with time in the next section.

5.2. Time-Evolution

The time-evolution of the cross-bandpass phases can be seen in Figure 7 for stations Mg, Oe, and Ow, and in Figure 8 for stations Wf, Ws, and Yj. Each panel corresponds to one VGOS band for one station, as indicated in the plot headings. The cross-bandpass phases are expressed in color and are plotted against time in the horizontal direction and against frequency in the vertical direction. The color bar is chosen such that −180° is red, −90° is green, 0° is blue, 90° is yellow, and +180° is red again, in order to account for the 360° phase ambiguities. In this manner, the evolution of the cross-bandpasses can be traced over the duration of the session. In general, the cross-bandpasses remain fairly stable and any variability evolves smoothly. There is, however, one feature that disrupts this continuity, and these are three vertical stripes of sudden phase-jumps, occurring approximately at times 14:00, 14:45, and 15:15 UTC. All stations are affected by this phenomenon, except for Mg, where these stripes might just not be visible because of the sparsity of the observations past 14:00. The three stripes are most pronounced in bands A and C, but there are weaker features of this type at other bands too (e.g., in band D for Oe and

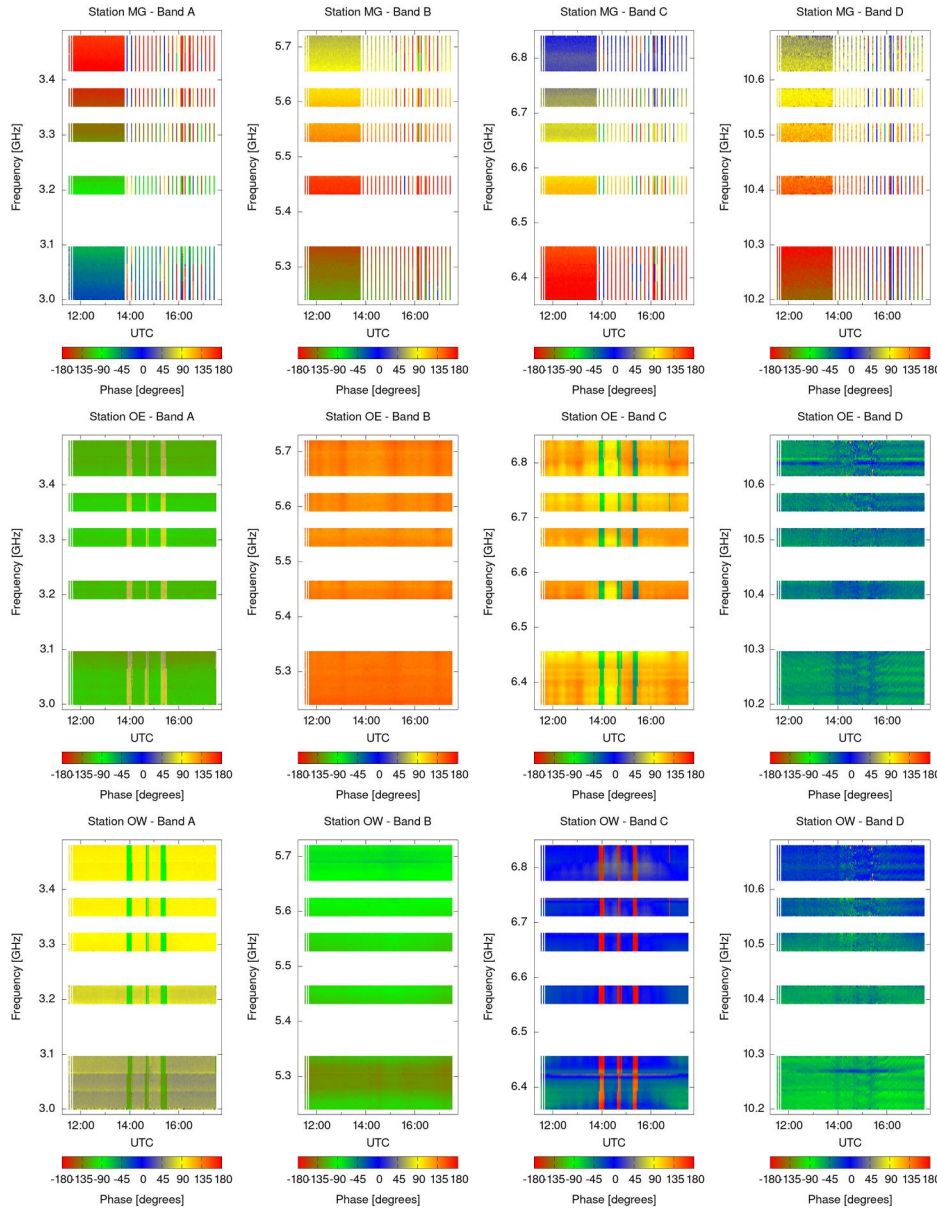

Figure 7. Time-evolution of the cross-bandpass phases, as color-coded, for stations Mg, Oe, and Ow.

Ow). Another remarkable characteristic of these features is that they seem to correspond to a sudden phase offset that remains rather stable in each of these three stripes, and seems to be the same for all three stripes in each band (meaning that the three stripes within each panel have the same color, but the colors in between panels differ). We tried to investigate the origin of these three stripes, but did not come to any definite conclusion. The first stripe coincides with missing data from station Wf at that time, and the second stripe with missing data from Yj for VGOS band A (cf. Figure 4). However, a solid causal relationship between the drop-out of a station and the occurrence of a stripe cannot be established, because there is not any such drop-out for the third stripe. During that time data from Mg are missing, but lack of data from that station does not lead to the appearance of any more stripes later on. For the remainder of our analysis, we treat the data from these stripes as outliers. The fact that such systematic corruption occurs is a matter of concern and the reasons should be clarification in a thorough future investigation.

Besides the three stripes, there is clearly a certain degree of variability of the cross-bandpasses. Evident examples of this are band C of both Onsala antennas and band D of the stations Westford and Wettzell. One possible reason

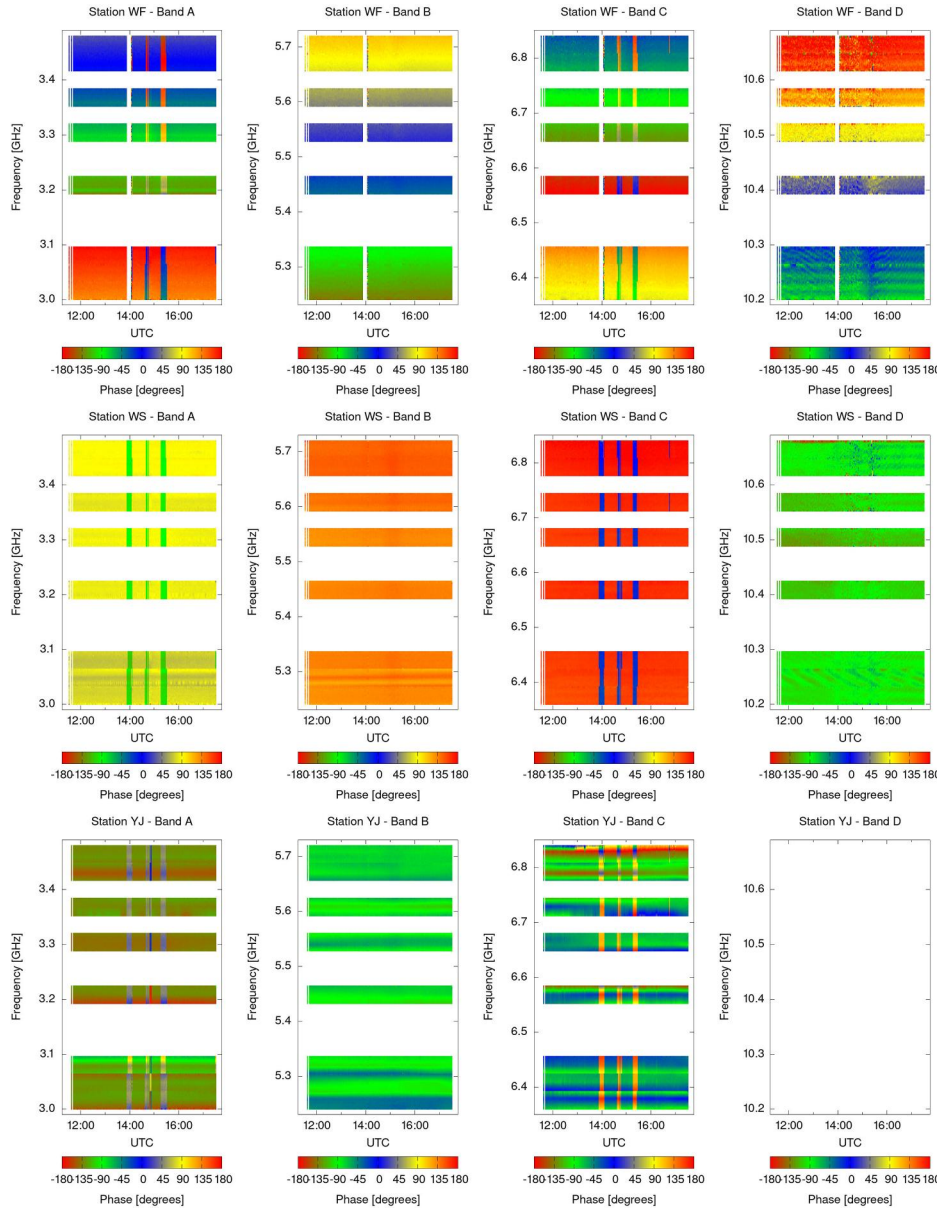

Figure 8. Same as Figure 7 but for stations Wf, Ws, and Yj.

for these smooth variability patterns is a variability in the phase-cal signal. This could be the case, because `PolConvert` takes as a first estimate of the cross-polarization phases the differences of the phases of the phase-cal signal. For this reason, we generated plots similar to Figures 7 and 8 but for the difference of the phases of the phase-cal signals. These plots are shown in Figures 9 and 10. There is indeed a certain similarity between the variability patterns of the phase-cal phases in band C of the two Onsala and the variability patterns of the cross-bandpasses. However, most of the time the phase-cal shows less variability than the cross-bandpasses. This is an indication that the cross-bandpasses themselves are indeed subject to some degree of variability with time.

We have carried out the same analysis for the cross-bandpass amplitudes, and the results are shown in Figures 11 and 12. There is not such a strong time-dependence of the amplitude ratios, compared to the phases. What becomes evident from these plots is a strong frequency dependency, which remains stable, to a certain degree, over the 6 hours of the experiment. That there can be considerable variability in time nevertheless shows the example of Yj, in the bottom row of Figure 12, at least in some of the sub-bands. Also Wf, in the top row,

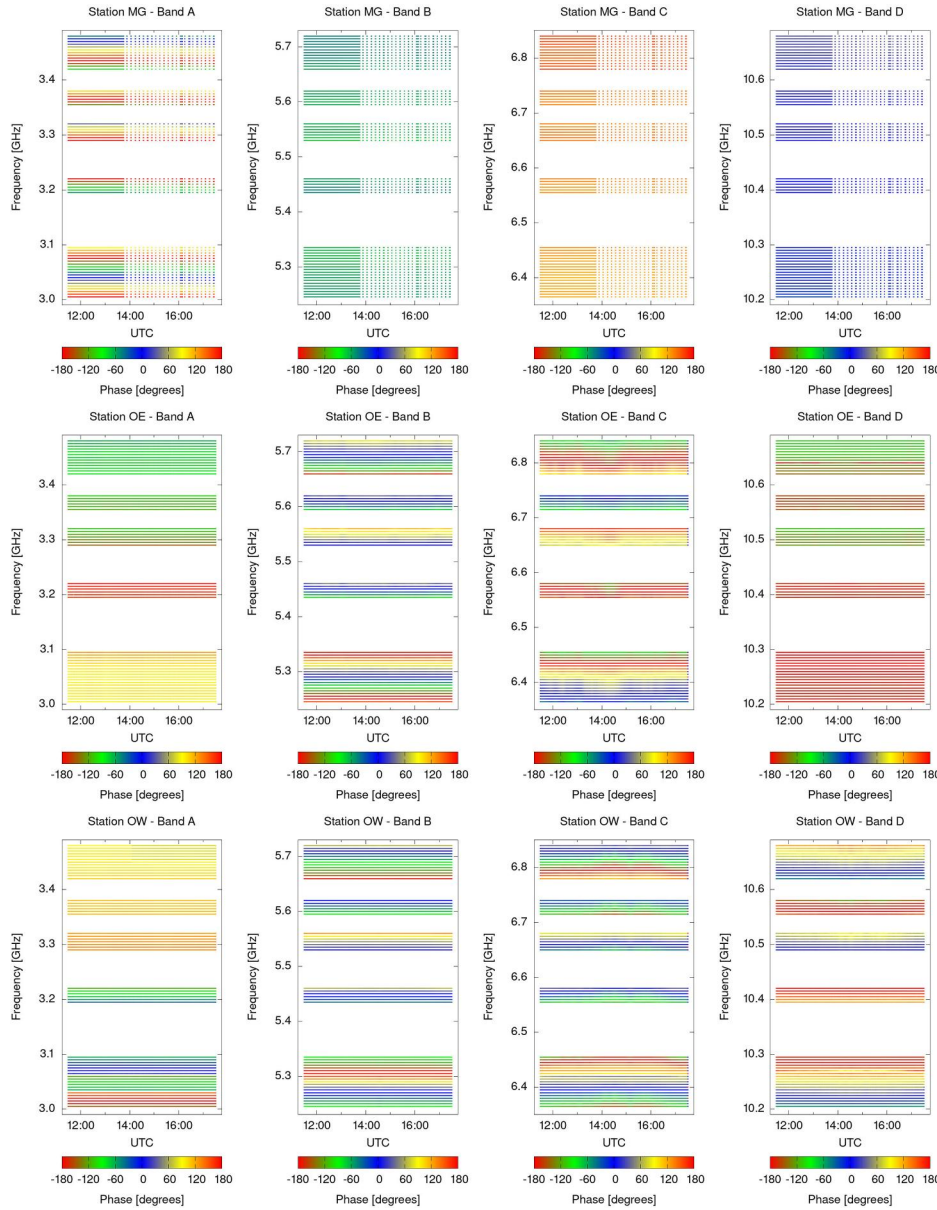

Figure 9. Time-evolution of the differential (H–V) phase-cal phases for stations Mg, Oe, and Ow.

shows rather sudden peaks in amplitude, some of which might be related to the three stripes that we saw in the phases.

Now we come back to station Ow and the time-evolution of the fit parameters of Equation 2 and Figure 6, where we noticed that the phase-frequency relationship is to first order characterized by a linear trend, that is, a group delay between the two linear polarizers within the same antenna. Here we repeat the fit of the function in Equation 2 and apply it to the entire data set to obtain a time series of the parameters τ and φ_0. We are applying this fit to the data of station Onsala West, which still serves as our example station. The result is plotted in Figure 13, where panels (a) and (b) show the time series of the group delay τ and the phase-offset φ_0, respectively. There is a high degree of correlation between these two parameters, which is in agreement with expectations because a change in the slope of a line inevitably changes the position of the intersection with the y-axis. In both plots (a) and (b) some outliers are clearly visible, and we highlighted them in red color. These outliers were identified by an eye-examination of the data, resulting in all data with $\tau > 240$ ps being rejected. The time of occurrence of these

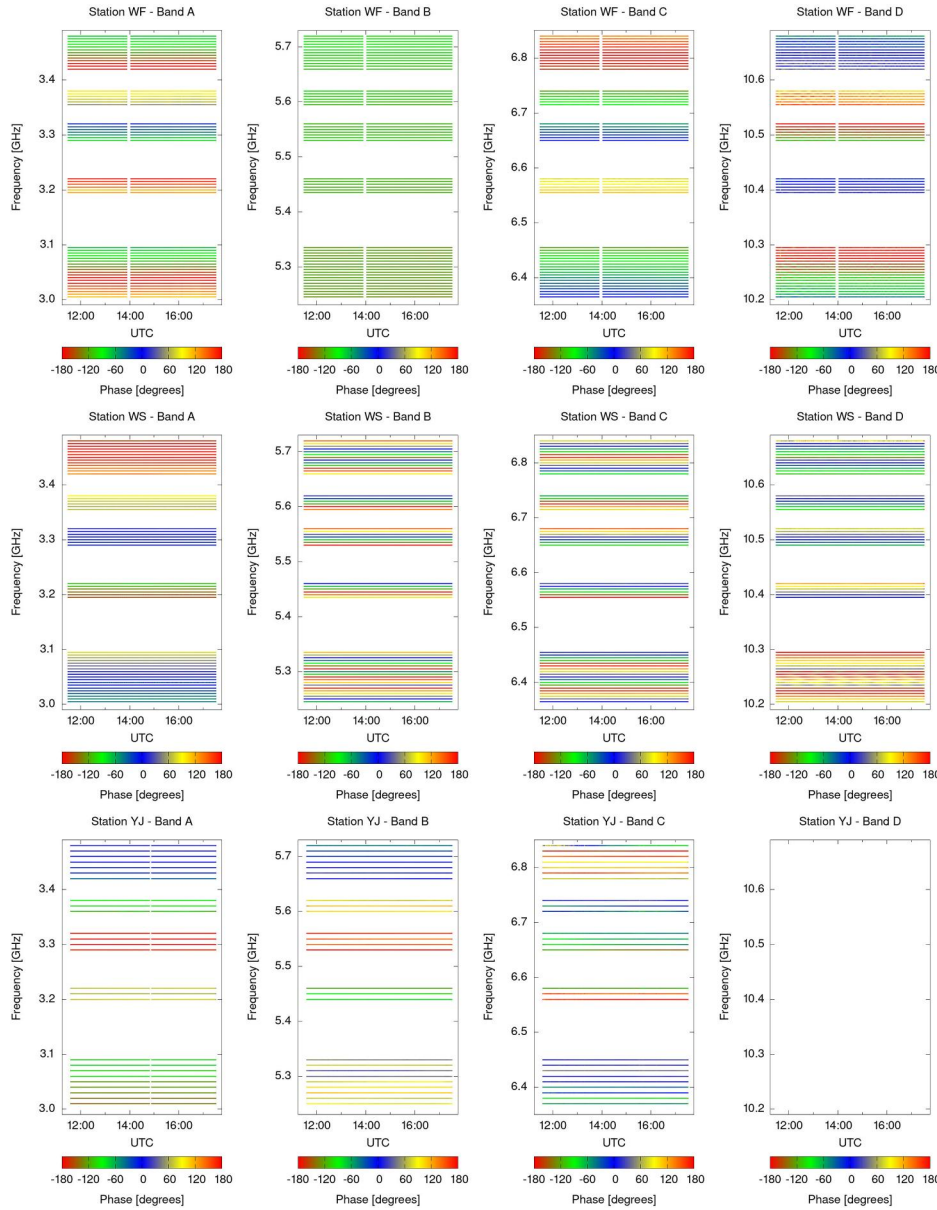

Figure 10. Same as Figure 9 but for station Wf, Ws, and Yj.

outliers coincides with the times of apparent disturbance, visible as the three vertical lines in the plots shown in Figures 7 and 8. We identify these outliers as the result of some corruption in our analysis and we will not include them in any further analysis. The black points in Figure 13a remain otherwise fairly stable with an average value of $\langle\tau\rangle = 230$ ps. However, already on this scale, a slight trend is also visible. The phase-offset in panel (b) shows a very similar picture. In order to investigate the variability of the group delay in more detail, we subtract the average value $\langle\tau\rangle$ from these data. The result is shown in Figure 13c. One can clearly see that there is variability of the group delay in the range of approximately -3 to $+3$ ps around the average value. This variability is not purely random, but there are clearly systematic trends visible. There seems to be a quasi-sinusoidal signal at the beginning of the time series until about 14:00 UTC, with the values oscillating around an otherwise stable mean. The period of this oscillation seems to be about half an hour. After that, the data seem to be dominated by an upward linear trend. Since these data are the result of tracking one single source, antenna elevation is a relatively simple function of time. This means the relationship between cross-polarization delay and time could as well be

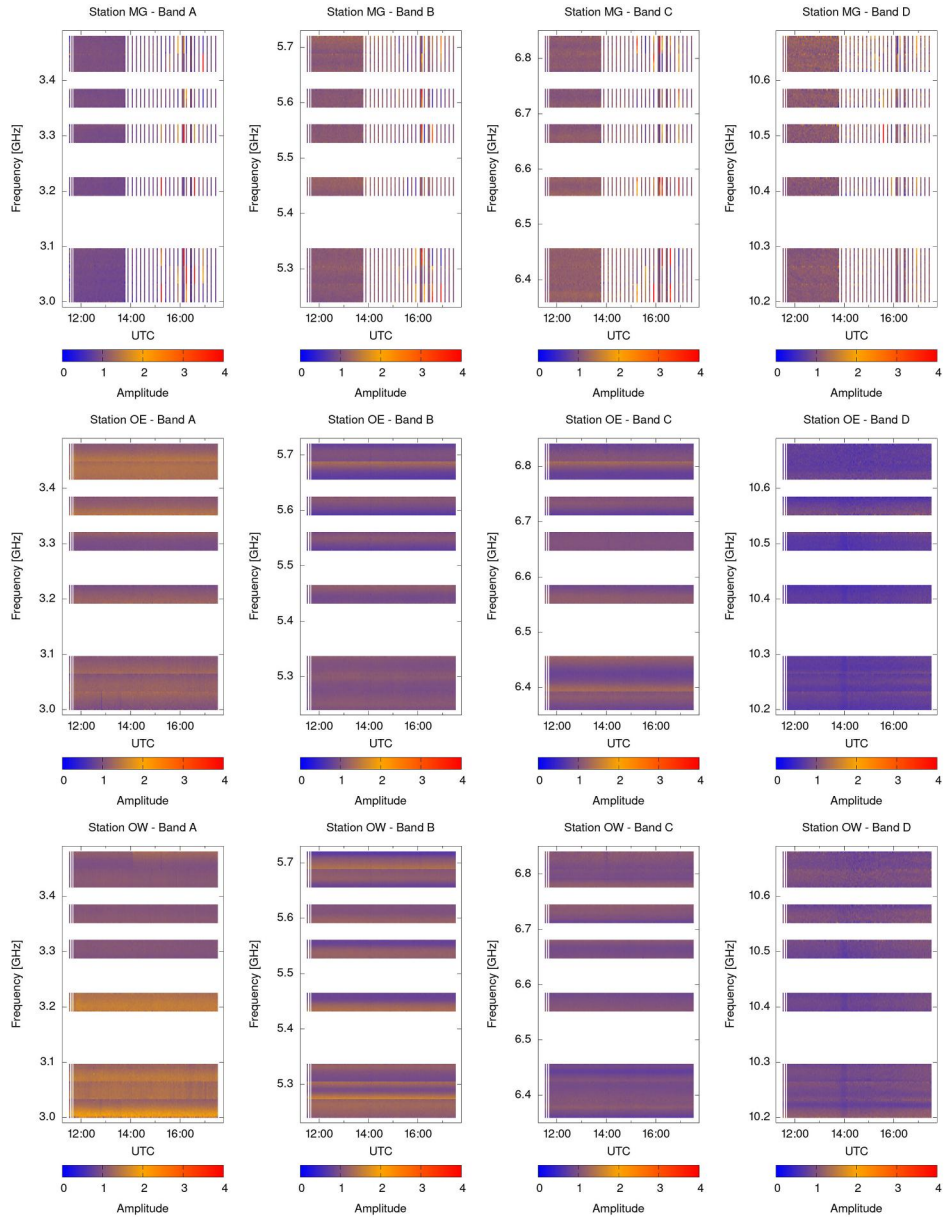

Figure 11. Time-evolution of the cross-bandpass amplitudes, as color-coded, for stations Mg, Oe, and Ow.

dependent on elevation. In this case, gravitational deformations of the instrument could play a role. It also is worth mentioning that the change in behavior at around 14:00 UTC coincides with the first occurrence of the disturbance, that is, the first of the three vertical lines in Figures 7 and 8.

5.3. Results for Sources NRAO 150 and OJ 287

At the beginning of the session er2201, we included two 5-min scans to two other sources. These sources were NRAO 150 and OJ 287, which we identified as potential cross-bandpass calibrators based on our experience from past experiments. We find that results obtained from observations of 4C 39.25 are still superior to those obtained from observations of these two other sources. This is visualized in Figure 14, where we show the phases of the cross-gain solutions for band A, sub-band 5, for the station Onsala West. Panel (a) shows the results for NRAO 150, (b) for OJ 287, and (c) for 4C 39.25. All three results were obtained from analyzing 2-min scans, cut from the original 5-min scans for NRAO 150 and OJ 287, and from the first 10-min scan of

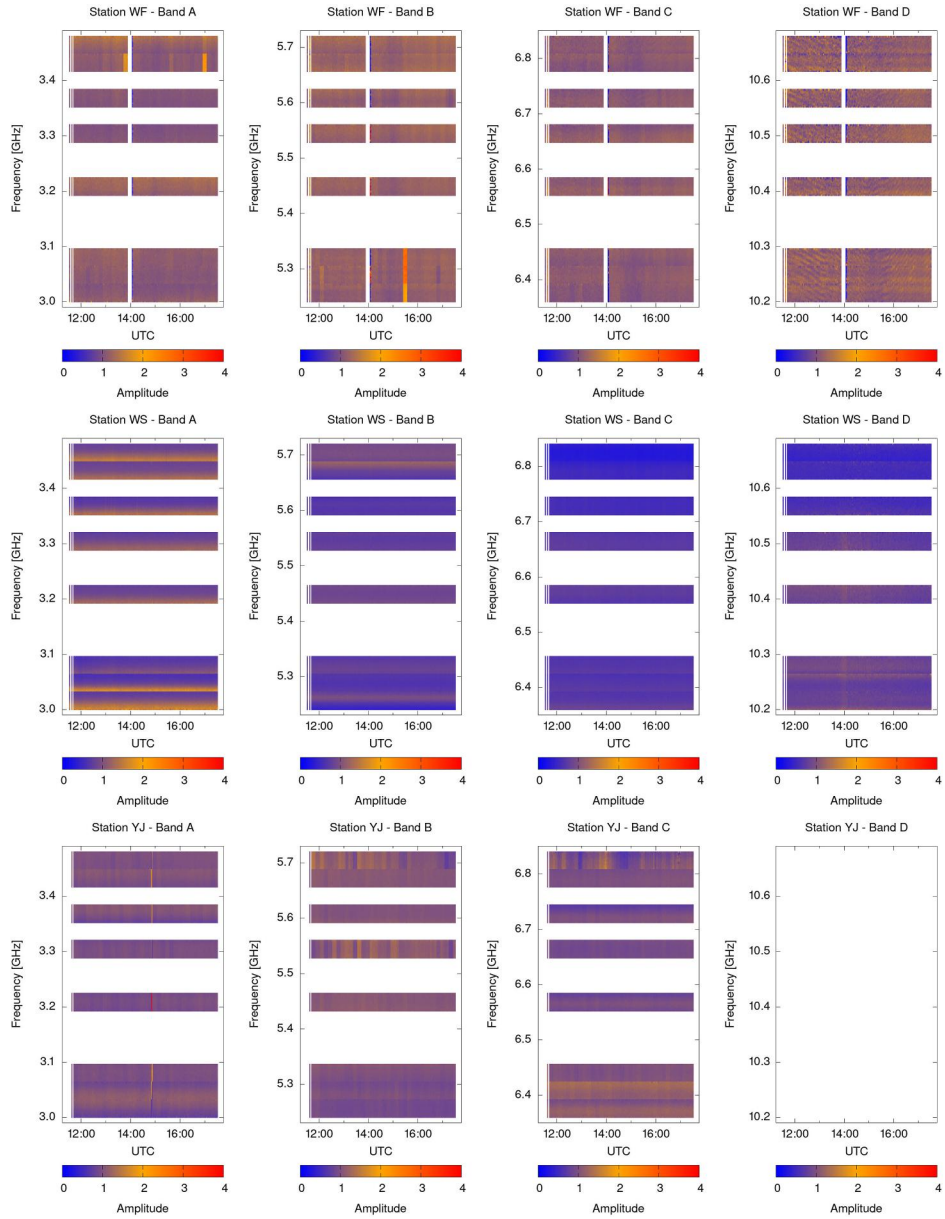

Figure 12. Same as Figure 11 but for stations Wf, Ws, and Yj.

4C 39.25. We turned off any frequency averaging in `PolConvert` because this allows to better see the signal-to-noise ratio. Time averaging was set to 20 s, as for the remainder of the results shown in this article. It is obvious by eye that the solution for 4C 39.25 looks much cleaner than the solutions for the two other sources. The phases obtained from both other sources are much noisier than those obtained from 4C 39.25. In addition to the noise, there are also systematic effects visible in the two other bandpasses, which are not present in panel (c). Both panels (a) and (b) show an effect that can be described as 180°-ambiguities, which correspond to a sign flip of the complex cross-gain values. In panel (c) the phase is basically stable at a value of ∼90°. In panels (a) and (b) the majority of the phases are scattered around 90°, but for some frequency intervals the phase is shifted to ∼−90°, that is, 180° downwards. In panel (a) this is visible at around 3.30 GHz and toward 3.32 GHz, and in panel (b) the phases cluster around −90° from the beginning of the sub-band until 3.30 GHz and around +90° from that point on until the end of the sub-band. These systematic offsets are not present at all in the solution obtained from 4C 39.25.

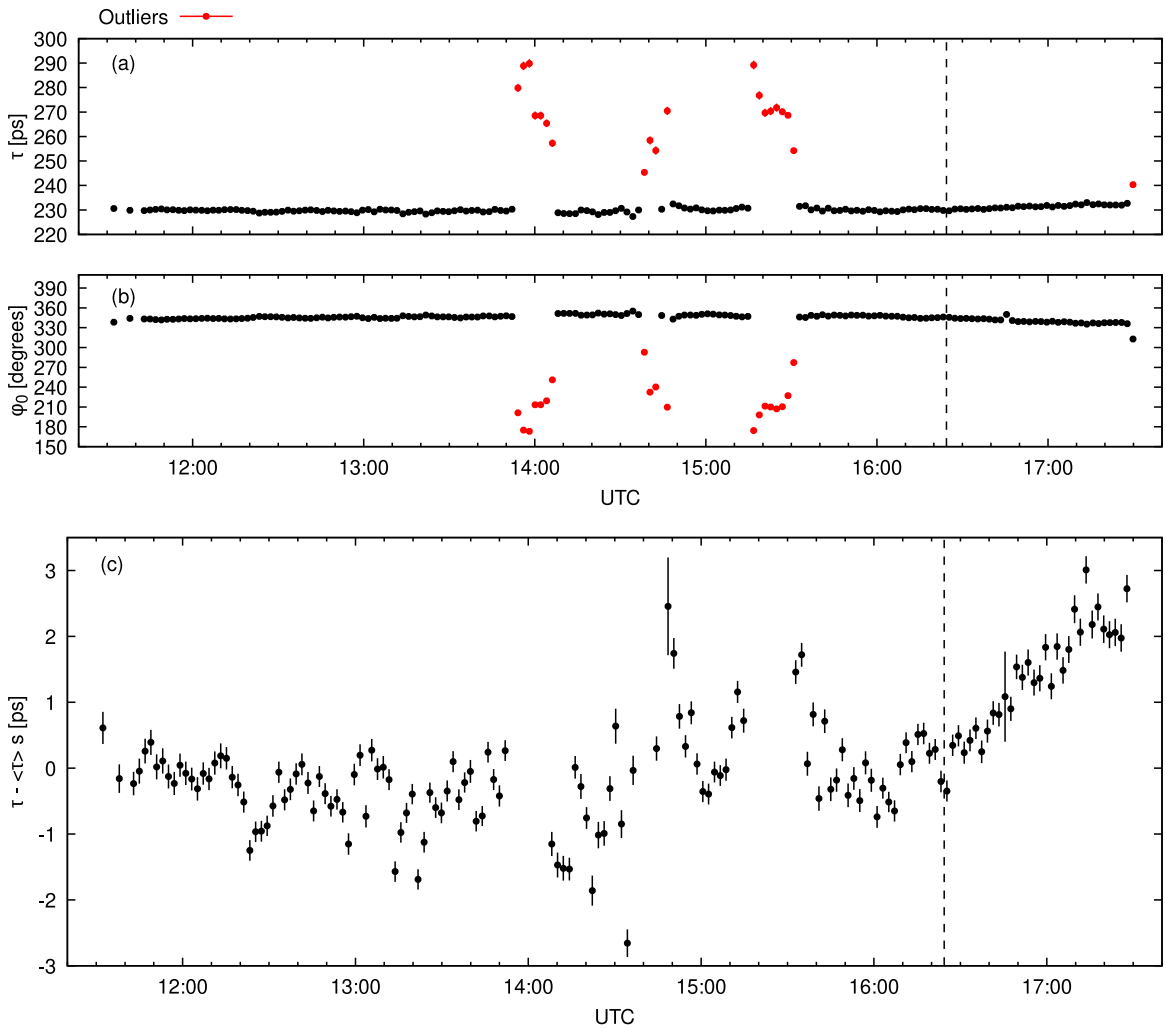

Figure 13. Time-evolution of the parameters obtained from fitting Equation 2 to the entire data set for station Ow. Outliers appear in red color and are not used for further analysis. The position of the reference scan 143 is marked by the vertical dashed line. (a) Group delay τ between H and V polarization. (b) Phase-offset φ_0. (c) Group delay τ with outliers removed and the average value of $\langle\tau\rangle = 230$ ps subtracted. Variability in the range ±3 ps can be seen along with some clearly systematic trends.

The results shown in Figure 14 and described here serve as an example to illustrate the superior quality of 4C 39.25 compared to other potential cross-bandpass calibrators, that have been investigated so far. They are representative of the results that we have obtained at other frequency ranges in this experiment and also in other experiments carried out in the past.

The suitability of 4C 39.25 as a calibrator might be surprising given the fact that it shows an extended VLBI morphology at cm wavelengths (as already pointed out in Section 2). The extended structure of this source is also mentioned in the context of the third realization of the international celestial reference frame (ICRF3) (Charlot et al., 2020). In ICRF2 (Fey et al., 2015) it was even treated as a "special handling source", as a consequence of its temporal source position variability, showing that its radio morphology is even subject to considerable changes over time. The concept of special handling source was abandoned in ICRF3. In the discussion of these issues it is important to point out that the quantities which are estimated by PolConvert in the analysis presented in this article, that is, the cross-polarization gains, are not affected by source structure, as long as the structure is not polarized. Only the polarized part of the radio source structure would affect the estimation of the cross-polarization gains.

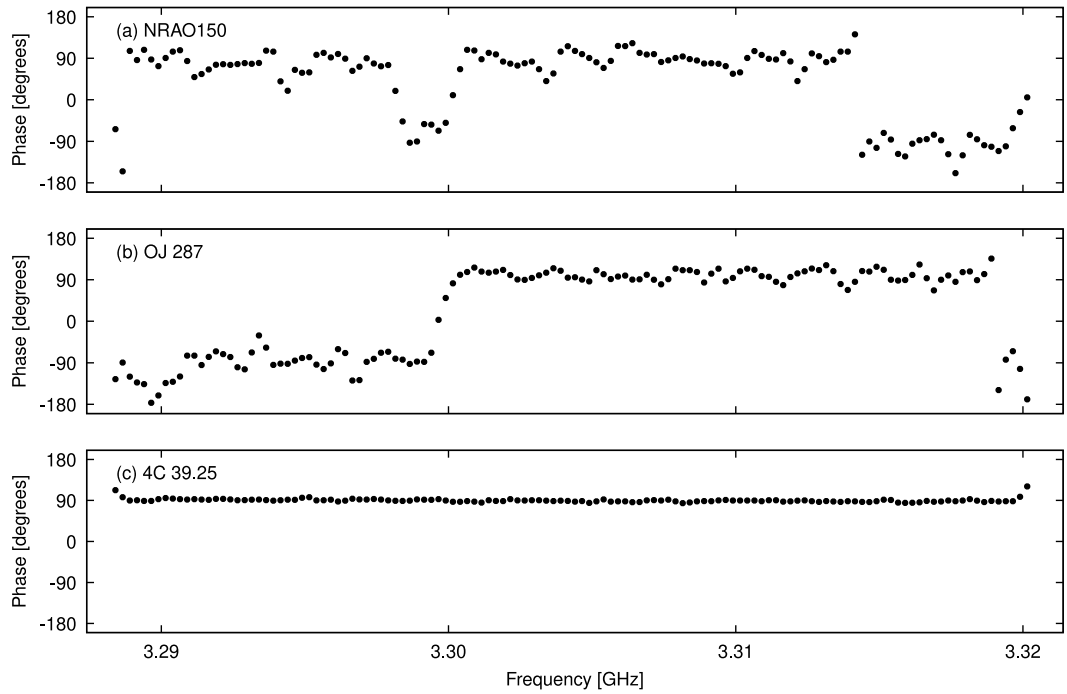

Figure 14. Cross-polarization bandpasses obtained from observations of (a) NRAO 150, (b) OJ 287, and (c) 4C 39.25. The three results were obtained from 2-min scans. The superior quality of 4C 39.25 is evident.

5.4. Long-Term Cross-Bandpass Stability

One of the aims of experiment er2201 was to investigate the time-evolution of VGOS cross-bandpasses over the duration of six hours. Here we discuss the long-term stability of cross-bandpasses over time scales of years. For this purpose, we make use of observations of 4C 39.25 in previous EU-VGOS (Albentosa et al., 2023, and references therein) sessions. The source was observed in the following sessions: ev9189, ev9203, ev9217.

Figure 15 shows the cross-bandpass solutions for Onsala West from observations of 4C 39.25 in sessions ev9189 (top panel, observed on 8 July 2019), ev9203 (middle panel, 22 July 2019), and ev9217 (bottom panel, 5 August 2019). First of all, in all three panels, the value of the overall group delay is similar, within a range of a few picoseconds. The exact estimates of the cross-polarization delays are listed in Table 4, where we also include a value for the session er2201. There is, however, an important difference between the first three and the last delay value in this table. While the first three values are derived from single scans, the value for er2201 is the average value (230 ps) of all delays plotted in Figure 13a, excluding the outliers. Because, as evident from Figure 13c, the scatter of the delays is not dominated by Gaussian noise but rather shows clear systematics, we do not report the uncertainty of the mean value (which is 1 ps) but instead the range of values that we see in this figure, that is, ±3 ps. The similarity of all four values is an indication that the delay between the two polarizers within one antenna can remain remarkably stable, even over a time span of several years, to within a few picoseconds.

However, there is also a component of the cross-polarization bandpasses that is considerably variable over timescales of years, and these are the residuals after subtracting the group delay. These residuals are shown in the lower panels in Figure 15. These variations are sometimes larger than the intrinsic scatter of the data points, as visible for example, in the uppermost residual plot in the figure (referring to ev9189). This is an indication that these variations can be significant.

6. Conclusions

In this article, we presented the results from a six-hour VLBI (VGOS) session consisting of cross-polarization bandpass calibrator scans of the source 4C 39.25. These are our conclusions:

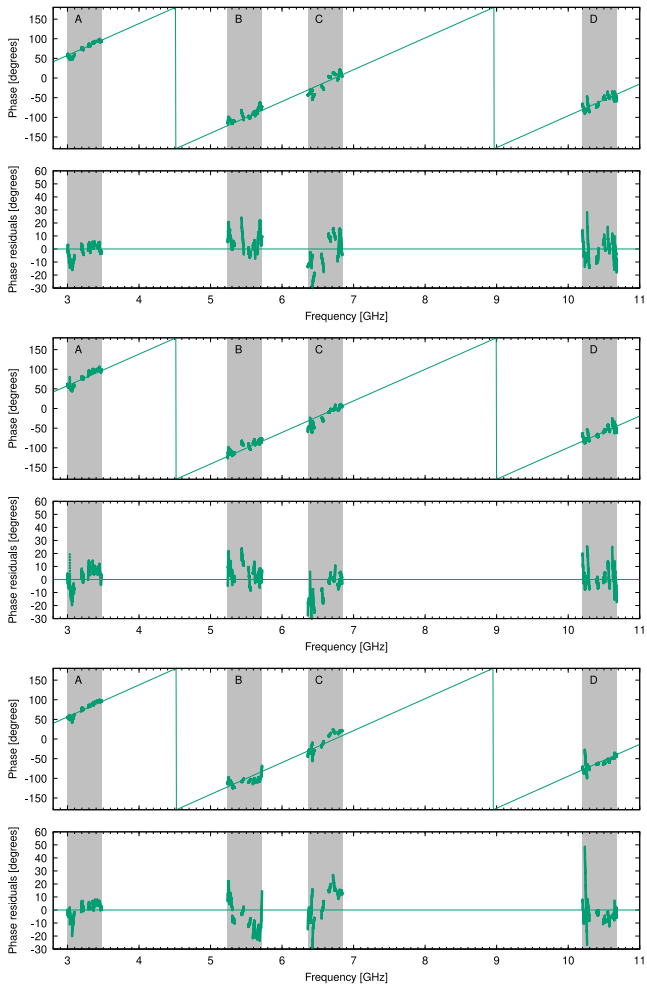

Figure 15. Cross-bandpass solutions for Onsala West from observations of 4C 39.25 in other EU-VGOS sessions. Top: ev9189, scan 115. Middle: ev9203, scan 115. Bottom: ev9217, scan 115.

1. The radio-loud AGN 4C 39.25 is confirmed as an excellent calibrator for the measurement of cross-polarization bandpasses of linearly polarized radio telescopes. Observations of this source still lead to the cleanest measurements that we have seen so far, compared to other sources (e.g., Figure 14). This statement is based on observations between 3 and 11 GHz. The suitability as a calibrator at other frequencies (e.g., mm wavelengths) should be subject of a future investigation.
2. We measured the cross-bandpasses for the VGOS antennas Mg, Oe, Ow, Wf, Ws, and Yj. The phases are to first order characterized by a group delay in the ∼100 ps regime, which remains stable over the six hours of the experiment with a variability of a few picoseconds. In our example, the remaining temporal variability of this delay is clearly characterized by systematic trends like oscillations and linear drifts (Figure 13c).
3. After removing a linear trend (i.e., group delay) from the cross-polarization phases, there is still considerable scatter as a function of frequency. In the time-domain, these phase-residuals show systematic and smooth transitions over the course of 6 hours of the experiment (cf. Figures 7 and 8).
4. Investigation of the long-term evolution of the cross-polarization delays shows that the delay can remain stable, but that the phase-scatter on top of the delay is still significantly variable (see Figure 15 and Table 4).
5. The cross-bandpass amplitudes are not constant over sub-bands, but show distinct shapes in frequency. This frequency-dependency has to be taken into account in cross-bandpass calibration.

The results obtained in our investigation can be useful for the adjustment of calibration strategies of VGOS sessions and other VLBI experiments including stations observing with linear feeds. These results show that cross-polarization bandpasses change systematically with time. This means that taking the average, for example, over one VGOS session is, stricly speaking, not valid. The underlying systemics can be removed from the data by applying a time-dependent calibration. We recommend including dedicated calibration scans in VGOS schedules. Two-minute scans of 4C 39.25 can be used for an improved calibration of VGOS data, which has in turn the potential of increasing the signal-to-noise ratio of databases and geodetic and astrometric results. It might be beneficial to update the cross-bandpasses multiple times per session, with a cadence of once per hour. In any case, it is highly recommended to include multiple calibrator scans for the sake of redundancy, because as we have seen here, calibration can at times be subject to corruption (see the three stripes in Figures 7 and 8). The exact impact, which the systematic cross-bandpass variability and its correction may have on the subsequent analysis should be the subject of a future investigation. Concerning the magnitude of the corrections, geophysical models and interpretations have improved down to the millimeter over the last decade. This is discussed, for example, in the context of the lastest realization of the International Terrestrial Reference Frame (ITRF2020) (Altamimi et al., 2023, and references therein). This means that the quality of the observations needs to be maintained at the same level, that is, ∼3 ps., which matches the magnitude of the systematic variability of the cross-polarization delay reported here.

Table 4
Cross-Polarization Delay Estimates Derived From Observations of 4C 39.25 in Different Sessions

Date (MM/DD/YYYY)	Session name	Delay [ps]
07/08/2019	ev9189	223.5 ± 0.3
07/22/2019	ev9203	224.3 ± 0.3
08/08/2019	ev9217	228.4 ± 0.4
09/08/2022	er2201	230 ± 3

Note. Concerning the delay uncertainties, for the first three sessions these are the nominal uncertainties from the least squares fit to a single scan, for session er2201 this is the range of values that we see in Figure 13.

Calibrator scans are optimized for the purpose of estimating parameters that are intrinsic to the instrument, this article focusing on the example of cross-polarization gains. In this respect, calibrator scans are useful for removing systematic errors from the data and also increase the signal-to-noise ratio. As a consequence, calibration has the positive effect of improving the accuracy of parameters of interest, estimated during the analysis of the session. Calibrator scans are, however, not necessarily optimized to be directly useful, by

themselves, for the estimation of these parameters. The following elaborates on potential deteriorating effects which the inclusion of calibration scans might have on the analysis of the session. The inclusion of calibrator scans into geodetic/astrometric VLBI sessions comes at the prize of reducing the observing time spent on scans that are optimized for the actual purpose of the experiment. One important aspect in this context is sky-coverage, which is crucial for the estimation of tropospheric parameters. VGOS sessions including one two-minute calibrator scan per hour have already been observed, and the effect of scan loss due to additional calibrator scans is marginal. Current VGOS schedules contain about 100 scans per hour, that is, approximately one scan every 36 s. Including one 120-s scan per hour would potentially mean a loss of three regular scans per hour, that is, three per cent of all scans of the session. This loss is not significant for the following reasons. In practice, current VGOS sessions are subject to technical problems that cause a scan loss rate that is already significantly higher than three per cent. This scan loss has not resulted in any significant degradation of the tropospheric estimation. In any case, a carefully prepared schedule will include the calibration scans in such a way that the degradation of sky-coverage will be kept to a minimum. The current 100 scans per hour leave a lot of headroom for the present parametrization of the analysis of VGOS sessions, also for the estimation of the other parameters of interest. In summary, in a carefully prepared schedule, the positive effects of the calibration will outweigh the marginal effects of scan loss.

The question of what it is that makes 4C 39.25 such an outstanding calibrator for the purpose of the measurement of linear cross-polarization bandpasses will be subject of a future investigation. Certainly, 4C 39.25 is one of the brightest AGN in the radio sky. However, we have the strong impression that brightness is not the only characteristic that sets this source apart, because observations of similarly bright sources have, so far, not given any similarly good results. The analysis of a dedicated survey of a large number of candidate sources will help to answer this question and increase the number of useful calibrators. An investigation of this nature is currently in progress and will be presented in a future publication.

Acronyms

AGN	Active Galactic Nucleus
ALMA	Atacama Large Millimeter/submillimeter Array
HOPS	Haystack Observatory Postprocessing System
IONEX	IONospheric map EXchange
MOJAVE	Monitoring Of Jets in Active galactic nuclei with VLBA Experiments
MIT	Massachusetts Institute of Technology
R&D	Research and Development
SNR	Signal-to-noise ratio
TEC	Total electron content
VLBA	Very Long Baseline Array
VLBI	Very Long Baseline Interferometry
VGOS	VLBI Global Observing System
VSC	Vienna Scientific Cluster

Data Availability Statement

The VLBI Level-1A correlator output data for the experiment er2201 can be obtained from NASA's crustal dynamics data information system (CDDIS, Noll, 2010) at https://cddis.nasa.gov/archive/vlbi/ivsdata/swin/2022/20220908_er2201_v001_swin.tar.bz2 (CDDIS, 2023). Registration is necessary. If you use these data for publication, please acknowledge the CDDIS and the IVS (Nothnagel et al., 2017). DiFX is available at https://www.atnf.csiro.au/vlbi/dokuwiki/doku.php/difx/installation along with installation instructions. The PolConvert software has been published on the Zenodo repository (Martí-Vidal et al., 2024).

Acknowledgments
We thank Sergio Dzib from the MPIfR for carefully reading the manuscript, and Inmaculada Malo-Gómez from Yebes Observatory for useful discussions about hybrid couplers. This research made use of data obtained from observations carried out by the International VLBI Service (Nothnagel et al., 2017). The computational results presented have been achieved in part using the Vienna Scientific Cluster (VSC). This research was funded in whole, or in part, by the Austrian Science Fund (FWF) [P 35920]. For the purpose of open access, the author has applied a CC BY public copyright licence to any Author Accepted Manuscript version arising from this submission.

References

Abdalmalak, K. A., Santamaría-Botello, G., Llorente-Romano, S., Rivera-Lavado, A., Flygare, J., Lopez Fernandez, J., et al. (2020). Ultra-wideband conical log-spiral circularly polarized feed for radio astronomy. *IEEE Transactions on Antennas and Propagation*, *68*(3), 1995–2007. https://doi.org/10.1109/TAP.2019.2949700

Albentosa, E., Alef, W., Bernhart, S., Böhm, J., Bolaño González, R., Choi, Y. K., et al. (2023). Current status of the EU-VGOS project. In K. L. Armstrong, D. Behrend, & K. D. Baver (Eds.), *International VLBI service for geodesy and astrometry 2022 general meeting proceedings* (pp. 85–89).

Alberdi, A., Gómez, J. L., Marcaide, J. M., Marscher, A. P., & Pérez-Torres, M. A. (2000). 4C 39.25: Witnessing the interaction between a moving and a stationary component. *Astronomy & Astrophysics*, *361*, 529–534.

Alef, W., Anderson, J. M., Bernhart, S., de Vicente, P., González García, J., Haas, R., et al. (2019a). The EUropean-VGOS project. In R. Haas, S. Garcia-Espada, & J. A. López Fernández (Eds.), *Proceedings of the 24th European VLBI group for geodesy and astrometry working meeting* (Vol. 24, pp. 107–111).

Alef, W., Tuccari, G., Dornbusch, S., Roy, A. L., Wunderlich, M., Kasemann, C., et al. (2019). Brand – A wideband receiver for astronomy and geodesy. In R. Haas, S. Garcia-Espada, & J. A. López Fernández (Eds.), *Proceedings of the 24th european VLBI group for geodesy and astrometry working meeting* (Vol. 24, pp. 31–36).

Aller, H. D. (1970). The polarization of variable radio sources at 8 GHz. I. The observations. *The Astrophysical Journal*, *161*, 1. https://doi.org/10.1086/150508

Altamimi, Z., Rebischung, P., Collilieux, X., Métivier, L., & Chanard, K. (2023). ITRF2020: An augmented reference frame refining the modeling of nonlinear station motions. *Journal of Geodesy*, *97*(5), 47. https://doi.org/10.1007/s00190-023-01738-w

Berge, G. L., & Seielstad, G. A. (1969). Polarisation measurements of extragalactic radio sources at 3.12-CM wave-length. *The Astrophysical Journal*, *157*, 35. https://doi.org/10.1086/150047

Bignell, R. C., & Seaquist, E. R. (1973). Observations of the linear polarization of radio sources at 2.8 and 4.5 CM. *The Astronomical Journal*, *78*, 536. https://doi.org/10.1086/111454

CDDIS. (2023). International VLBI service for geodesy and astrometry (IVS) VLBI level 1A correlator output [online]. NASA crustal dynamics data information system daac, Greenbelt, MD, USA. https://doi.org/10.5067/VLBI/vlbi_l1a_swin_001

Charlot, P., Jacobs, C. S., Gordon, D., Lambert, S., de Witt, A., Böhm, J., et al. (2020). The third realization of the International Celestial Reference Frame by very long baseline interferometry. *Astronomy & Astrophysics*, *644*, A159. https://doi.org/10.1051/0004-6361/202038368

Deller, A. T., Brisken, W. F., Phillips, C. J., Morgan, J., Alef, W., Cappallo, R., et al. (2011). DiFX-2: A more flexible, efficient, robust, and powerful software correlator. *Publications of the Astronomical Society of the Pacific*, *123*(901), 275–287. https://doi.org/10.1086/658907

Event Horizon Telescope Collaboration, Akiyama, K., Alberdi, A., Alef, W., Asada, K., Azulay, R., et al. (2019). First M87 event horizon telescope results. I. The shadow of the supermassive black hole. *The Astrophysical Journal*, *875*(1), L1. https://doi.org/10.3847/2041-8213/ab0ec7

Fey, A. L., Gordon, D., Jacobs, C. S., Ma, C., Gaume, R. A., Arias, E. F., et al. (2015). The second realization of the international celestial reference frame by very long baseline interferometry. *The Astronomical Journal*, *150*(2), 58. https://doi.org/10.1088/0004-6256/150/2/58

García-Pérez, O., Terceroc, F., Malo, I., Gallego, J. D., & López-Pérez, J. A. (2018). *Linear to circular polarization conversion using microwave hybrids for BRAND (1.5–15.5 GHz)* (CDT Technical Report No. 2018-12). Observatorio de Yebes Guadalajara (Spain).

García-Pérez, O., Terceroc, F., Malo, I., & López-Pérez, J. A. (2018). *Linear to circular polarization conversion using microwave hybrids for VGOS (2–14 GHz)* (CDT Technical Report No. 2018-13). Observatorio de Yebes Guadalajara (Spain).

Impey, C. D., & Tapia, S. (1990). The optical polarization properties of quasars. *The Astrophysical Journal*, *354*, 124. https://doi.org/10.1086/168672

Jaradat, A., Jaron, F., Gruber, J., & Nothnagel, A. (2021). Considerations of VLBI transmitters on Galileo satellites. *Advances in Space Research*, *68*(3), 1281–1300. https://doi.org/10.1016/j.asr.2021.04.048

Jaron, F., Bernhart, S., Böhm, J., González García, J., Gruber, J., Choi, Y. K., & EU-VGOS Collaboration. (2021). EU-VGOS activities in Vienna. In R. Haas (Ed.), *25th European VLBI group for geodesy and astrometry working meeting* (Vol. 25, pp. 19–23).

Khudchenko, A., Fominsky, M., Heiter, C., Heyminck, S., Gusten, R., Klein, B., et al. (2019). Design and performance of a sideband separating SIS mixer for 800–950 GHz. *IEEE Transactions on Terahertz Science and Technology*, *9*(6), 532–539. https://doi.org/10.1109/TTHZ.2019.2939003

Kooi, J., Soriano, M., Bowen, J., Abdulla, Z., Samoska, L., Fung, A., et al. (2023). A multioctave 8 GHz–40 GHz receiver for radio astronomy. *IEEE Journal of Microwaves*, *3*(2), 570–586. https://doi.org/10.1109/JMW.2023.3237693

López-Pérez, J. A., Tercero-Martínez, F., Serna-Puente, J. M., Vaquero-Jiménez, B., Patino-Esteban, M., García-Carreño, P., et al. (2021). A tri-band cooled receiver for geodetic VLBI. *Sensors*, *21*(8), 2662. https://doi.org/10.3390/s21082662

Malo-Gomez, I., Gallego-Puyol, J. D., Diez-Gonzalez, C., Lopez-Fernandez, I., & Briso-Rodriguez, C. (2009). Cryogenic hybrid coupler for ultra-low-noise radio astronomy balanced amplifiers. *IEEE Transactions on Microwave Theory and Techniques*, *57*(12), 3239–3245. https://doi.org/10.1109/TMTT.2009.2033874

Martí-Vidal, I., Crew, G. B., Reynolds, C., Marcote, B., & Kettenis, M. (2024). marti-vidal-i/polconvert: Version 2.0.7 – Vgos. Zenodo. https://doi.org/10.5281/zenodo.10818913

Martí-Vidal, I., Mus, A., Janssen, M., de Vicente, P., & González, J. (2021). Polarization calibration techniques for the new-generation VLBI. *Astronomy & Astrophysics*, *646*, A52. https://doi.org/10.1051/0004-6361/202039527

Martí-Vidal, I., Roy, A., Conway, J., & Zensus, A. J. (2016). Calibration of mixed-polarization interferometric observations. Tools for the reduction of interferometric data from elements with linear and circular polarization receivers. *Astronomy & Astrophysics*, *587*, A143. https://doi.org/10.1051/0004-6361/201526063

Nartallo, R., Gear, W. K., Murray, A. G., Robson, E. I., & Hough, J. H. (1998). A millimetre/submillimetre polarization survey of compact flat-spectrum radio sources. *Monthly Notices of the Royal Astronomical Society*, *297*(3), 667–686. https://doi.org/10.1046/j.1365-8711.1998.01405.x

Niell, A., Barrett, J., Burns, A., Cappallo, R., Corey, B., Derome, M., et al. (2018). Demonstration of a broadband very long baseline interferometer system: A new instrument for high-precision space geodesy. *Radio Science*, *53*(10), 1269–1291. https://doi.org/10.1029/2018RS006617

Noll, C. E. (2010). The crustal dynamics data information system: A resource to support scientific analysis using space geodesy. *Advances in Space Research*, *45*(12), 1421–1440. https://doi.org/10.1016/j.asr.2010.01.018

Nothnagel, A., Artz, T., Behrend, D., & Malkin, Z. (2017). International VLBI Service for Geodesy and Astrometry. Delivering high-quality products and embarking on observations of the next generation. *Journal of Geodesy*, *91*(7), 711–721. https://doi.org/10.1007/s00190-016-0950-5

Petrachenko, B., Niell, A., Behrend, D., Corey, B., Boehm, J., Charlot, P., et al. (2009). Design aspects of the VLBI2010 system. In *Progress report of the IVS VLBI2010 Committee, June 2009*. NASA/TM-2009-214180, 62 pages.

Pilkington, J. D. H., & Scott, J. F. (1965). A survey of radio sources between declinations 20° and 40°. *Memoirs of the Royal Astronomical Society*, *69*, 183.

Schartner, M., & Böhm, J. (2019). VieSched++: A new VLBI scheduling software for geodesy and astrometry. *Publications of the Astronomical Society of the Pacific*, *131*(1002), 084501. https://doi.org/10.1088/1538-3873/ab1820

Sovers, O. J., Fanselow, J. L., & Jacobs, C. S. (1998). Astrometry and geodesy with radio interferometry: Experiments, models, results. *Reviews of Modern Physics*, *70*(4), 1393–1454. https://doi.org/10.1103/RevModPhys.70.1393

Thompson, A. R., Moran, J. M., Swenson, J., & George, W. (2017). Interferometry and synthesis in radio astronomy (3rd ed.). https://doi.org/10.1007/978-3-319-44431-4

Zhao, G.-Y., Gómez, J. L., Fuentes, A., Krichbaum, T. P., Traianou, E., Lico, R., et al. (2022). Unraveling the innermost jet structure of OJ 287 with the first GMVA + ALMA observations. *The Astrophysical Journal*, *932*(1), 72. https://doi.org/10.3847/1538-4357/ac6b9c